NASA/CR—1998-206606

Dynamics of Large-Scale Structures for Jets in Crossflow

Frank Muldoon and Sumanta Acharya
Louisiana State University, Baton Rouge, Louisiana

Prepared for the
43rd Gas Turbine and Aeroengine Congress, Expo, and User's Symposium
sponsored by the International Gas Turbine Institute of
the American Society of Mechanical Engineers
Stockholm, Sweden, June 2–5, 1998

Prepared under Grant NAG3–1641

National Aeronautics and
Space Administration

Lewis Research Center

March 1998

Acknowledgments

This work was supported by a grant from the Turbomachinery Physics Group at NASA Lewis. Dr. Chi Wang and Dr. Ray Gaugler served as the technical monitors for the project. Their support is gratefully acknowledged. Computing support for the project was received from NASA Ames Computing Center and also through NASA Lewis. This support is also acknowledged. The assistance of Dr. Albert Harvey III and Raymond Jones at Dow Chemical Company is gratefully acknowledged.

Available from

NASA Center for Aerospace Information
800 Elkridge Landing Road
Linthicum Heights, MD 21090-2934
Price Code: A03

National Technical Information Service
5287 Port Royal Road
Springfield, VA 22100
Price Code: A03

DYNAMICS OF LARGE-SCALE STRUCTURES FOR JETS IN CROSSFLOW

Frank Muldoon* and Sumanta Acharya**
Mechanical Engineering Department
Louisiana State University
Baton Rouge, LA 70803

ABSTRACT

Results of a three dimensional unsteady computational study of a row of jets injected normal to a cross-flow are presented with the aim of understanding the dynamics of the large scale structures in the region near the jet. The jet to cross-flow velocity ratio is .5. A modified version of the computer program (INS3D) which utilizes the method of artificial compressibility is used for the computations. Results obtained clearly indicate that the near field large scale structures are extremely dynamical in nature, and undergo bifurcation and reconnection processes. The dynamical near field structures identified include the counter rotating vortex pair (CVP), the horse-shoe vortex, wake vortex, wall vortex and the shear layer vortex. The dynamical features of these vortices are presented in this paper. The CVP is observed to be a convoluted structure interacting with the wall and horse-shoe vortices. The shear layer vortices are stripped by the crossflow, and undergo pairing and stretching events in the leeward side of the jet. The wall vortex is reoriented into the upright wake system. Comparison of the predictions with mean velocity measurements is made. Reasonable agreement is observed.

*Graduate Student
**Professor, and Author to whom all correspondence should be addressed

INTRODUCTION

Jets in crossflow have been studied extensively due to potential applications in gas turbine blade cooling, control of pollutant discharges, roll-control of missiles, etc. The majority of these studies dealing with the details of the flow structure have been on single jets issuing into a crossflow. Early experimental studies dealt with experimental efforts to determine the mean flow behavior and pressure distributions (see for example, Kamotani and Gerber, 1972; and Andreopoulos, 1982; Andreopoulos and Rodi, 1984). Flow visualization studies have revealed the existence of several vortical structures, and have indicated the importance of their dynamical nature. The counter-rotating vortex pair (commonly referred to as the CVP) is reported to be the most dominant structure persisting far downstream of the jet injection. This is believed to be due to the vortex street exiting the injection hole and its reorientation by the crossflow (Foss, 1980; Andreopoulos, 1985; Kelso et al., 1996). In addition, shear layer or ring vortices, driven by Kelvin-Helmholtz instability, are generated in the near field of the jet. The adverse pressure gradient introduced by the jet blockage produces the horseshoe vortices (with spanwise vorticity) which are deflected and stretched by the crossflow, and these travel downstream (with streamwise vorticity) rotating in a direction opposite to the CVP. Finally upright wake vortices between the surface and the jet have been observed (see Fric and Roshko, 1994), and these have been attributed

to the separation of the crossflow boundary layer due to spanwise pressure gradients.

Computational studies aimed at examining the details of the flow structure have been relatively limited. The majority of the reported studies have primarily solved the Reynolds-Averaged-Navier-Stokes (RANS) equations, and due to the intrinsic time-averaging that is associated with these equations, the dynamical nature of the vortical structures can not be predicted. Further, turbulence models have to be introduced, and the accuracy of even the time-averaged calculations are themselves compromised by the validity of the model. Examples of RANS calculations are those of Patankar et al., (1977), Sykes et al. (1986), Kim and Benson (1992) and Demuren (1993). More recently, Jones (1996) and Yuan and Street (1996) presented Large Eddy Simulations (LES) that resolve the dynamics of the large scales and model the small scales, and observed some of the reported phenomena in the experiments.

The application of interest in the present paper is the film cooling of gas turbine blades. In this configuration, a row of coolant jets is injected into a hot crossflow. The coolant jets are usually injected at an angle to the main crossflow direction. The goal of the jets is to provide a wide coverage of the blade surface. This problem differs from the single-jet-in-crossflow studies, in that, the spanwise boundaries are no longer freestream boundaries. They are either periodic or symmetry (in a time averaged sense) boundary conditions. Further the length to diameter ratio of the injection hole is usually small (in the range of 1.5-5), and therefore the flow development in the injection hole is affected by the crossflow leading to a highly non-uniform jet-exit profile. This is in contrast to the single-jet studies where the hole exit profile has been assumed to be or is symmetrical. Since the vorticity exiting the hole has a very strong influence of the downstream development of the dynamical structures, appropriate specification of the jet-exit conditions are necessary.

In the near field of the film cooling jet, the dynamical large scale structures are likely to control the mixing process, as has been shown in free jet studies (see, for example, the review by Ho and Huerre, 1984) and it is this mixing that dictates the normal and transverse penetration of the jet. To accurately predict the heat transfer or the adiabatic effectiveness from the surface, it is important to correctly predict the jet penetration and reattachment, and for this the dynamics of the near field structures must be accurately simulated. This necessitates a time- and space-accurate calculation of the flow field (DNS or LES). However, while there are many computational studies dealing with film cooling predictions (see Garg and Gaugler, 1994, 1995), they are primarily limited to RANS based calculations and are therefore unable to predict the near-field evolution of the jet ($x/d<5$) very well. In this paper, we present time-and space accurate calculations for a typical film cooling configuration, with the specific intent of understanding the dynamics of the various vortical structures in the near-field. To the authors knowledge, direct numerical simulation (DNS) or LES for the film cooling configuration have not been reported.

PROBLEM DESCRIPTION

The physical configuration (Figure 1) chosen corresponds to an experimental study reported by Ajersch et al. (1995). The coolant jets are injected at 90 degrees (vertically upwards) from a square-cross-section inlet duct with an average velocity of 5.5m/s. The width of the square jet exit hole =d=12.7mm. The freestream value of the crossflow velocity is 11m/s. The measurements of Ajersch et al. (1995) are used for boundary conditions at both the crossflow inlet and the jet exit. In the experiments of Ajersch et al. (1995) the crossflow boundary layer approaching the jet was tripped by a thin rod to ensure a turbulent boundary layer. Both the jet and crossflow air are at the same (room) temperature. The Reynolds number based

on the jet diameter (d) and average jet velocity is 4700.

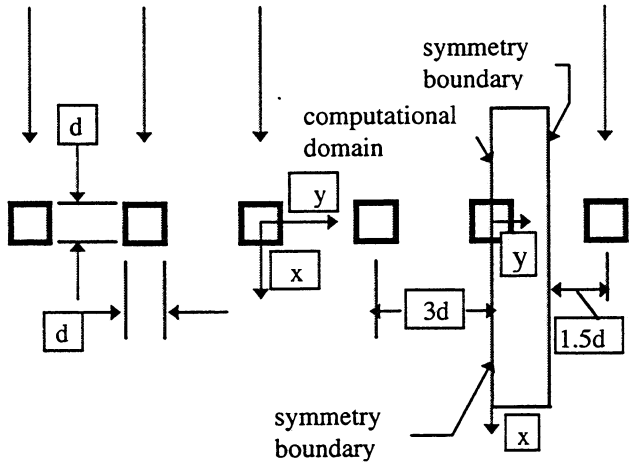

Figure 1 Diagram of the physical problem

Since the primary goal of the present study is to examine the *dynamics* of the large-scale vortical structures in the near-field, only a modest number of grid points (nearly 277,000) have been used in the present study. It is recognized that this mesh will be unable to resolve the dynamics of the small scale structures, nor the interaction between the small and large scales. With this in mind, no statistics, except mean velocity, are presented in this paper, and the discussion is focused on the dynamics of the near-field large scale structures. The experimental studies referenced earlier (Foss, 1980; Fric and Roshko, 1994; Kelso et al., 1996) clearly indicate that the near-field vortical structures are large scale events, controlled largely by inviscid phenomena, and that the small scale turbulence has little influence in this region. Therefore, it is expected that with the mesh used in the present calculations, the near-field dynamics would be correctly predicted.

Figures 2 and 3 show the computational domain. The computational domain extended from x/d=-6.3 to 12, y/d=0 to 1.5, z/d=0 to 4. A stretched Cartesian grid with 191 points in the x direction, 29 in the y and 50 in the z direction was used. The grid was fairly dense and uniform near the jet, from x/d=-0.5 to x/d=0.5, and y/d=0 to 0.5. In wall coordinates Δx^+ ranged from 20 near the jet to 60 well downstream, Δy^+ is nearly 20 across the whole spanwise direction, and Δz^+ ranged from about 8 near the wall to about 60 far away from the wall.

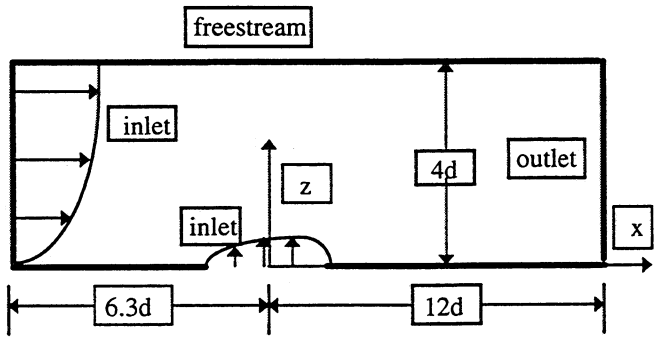

Figure 2 Diagram of the computational domain

At y/d=0 and y/d=1.5 symmetry boundary conditions were used. In order to accurately represent the inlet boundary conditions, perturbations were introduced at both the jet and cross flow inlet. This was accomplished by adding a fluctuating component of velocity to the mean velocity data of Ajersch et al. (1995). The fluctuating component $F(j,k,t)$ is specified by eqn. (1) and is composed of 10 frequencies. The numbers a and b are generated randomly between 0 and 1. The effect of b, which is a function only of the gridpoints, is to provide a different phase shift for every spatial location. The term A was chosen to control the amplitude of the perturbations to match that of the experimental data of Ajersch et al. (1995).

$$F(j,k,t) = A(j,k)\sum_{n=1}^{10}\sin(f(n)*(1+.015*(a(j,k,t)-.5))*t+b(j,k)) \quad (1)$$

The frequencies at which the flow was perturbed ranged from 1.2 to 36 Hz. The computed dominant frequencies of the flow were in the range 100-200 Hz. This implies that the natural instabilities were

established in the flow, and were not influenced by the frequencies introduced at the boundaries.

SOLUTION METHOD

The three dimensional unsteady incompressible Navier-Stokes equations are solved by the method of artificial compressibility, which was first suggested by Chorin (1968). In this method the incompressible Navier-Stokes equations are modified by the addition of a derivative of (pressure times a constant) with respect to a psuedotime to the continuity equation. This creates a situation similar to that of the compressible Navier-Stokes equations in which the effect of pressure appears in the continuity equation due to the presence of a derivative of density with respect to time. This enables the incompressible Navier-Stokes equations to be solved using methods derived for the compressible Navier-Stokes equations. When steady state is reached in psuedotime the added term in the continuity equation becomes zero and the incompressible continuity equation is satisfied. Real time solutions are obtained by adding the appropriate terms to the steady state incompressible Navier-Stokes equations and obtaining a steady state solution in psuedotime for each real time step. We use a code called INS3D which was developed at NASA Ames Research Center by Rogers and Kwak et al (1989). This code incorporates a 3rd and a 5th order upwind representation for the convective terms along with a 2nd order central difference representation for the diffusion terms. All calculations presented in this paper were done using the 3rd order upwind representation for the convective terms. We have modified the code to use a 4rth order central difference representation for the diffusion terms. A 2nd order representation is used for the temporal terms. The code is capable of handling generalized curvilinear coordinates. We have changed the differencing of the metric terms from 2nd order accuracy to a user defined arbitrary order of accuracy utilizing Fornberg's algorithm Fornberg (1988). In our calculations we use 4rth order accurate representations for the metric terms. Between 40 and 45 subiterations were needed to move one physical time step. Eight hours on a Cray C90 were required to move approximately 68 time steps. The solution was advanced over 1700 time steps. This corresponds to a particle passing through the computational domain 12 times based on the jet velocity.

RESULTS AND DISCUSSIONS

Main Features at One Time Instance

Figure 3 shows the instantaneous values of the x-vorticity at three different x-y planes above the surface. Above the surface (z/d >.137), the dominant features of the flow field are the horseshoe vortex (positive vorticity) and the CVP (negative vorticity). The horseshoe vortex system grows both in the spanwise and vertical direction as it develops downstream. At a vertical location corresponding to z/d= .137, a splitting of the horseshoe vortex system is noted, with one leg traveling downstream along the symmetry boundary, and the other being entrained into the wake of the jet (by x/d=2). This bifurcation process repeats itself further downstream (by x/d=4 and again by x/d=6). In the near field (x/d=2), the entrained positive vorticity convolutes the CVP, and as a consequence, the instantaneous flow field consists of a highly stretched and distorted CVP (negative vorticity) with pockets of positive vorticity. The positive vorticity, particularly close to the wall, is also caused by the wall vortex, as discussed in the next paragraph.

At the surface (z/d=0), negative vorticity is noted directly below the footprint of the horseshoe vortex, while positive vorticity is noted on the leeward side of the injection hole. The low pressure in the wake region produces the pressure defect responsible for driving the exiting jet flow in the spanwise direction producing vorticity counter to the horseshoe vortex. Examination of the instantaneous pressure contours at the same time-instance (Fig. 4) indicates both axial and spanwise pressure gradients along the transverse edge of the

jet which are responsible for a thin flow-stream from the transverse edge of the jet, with positive vorticity, to be directed toward the jet symmetry plane. This is akin to the wall-vortex behavior observed by Kelso et al. (1996) where the flow bifurcates towards the jet center-plane from a saddle point on the transverse side and encounters an adverse pressure gradient near the centerline causing flow separation and a wall vortex system. Contours of the x-vorticity in cross-stream planes will later show time instances in which this positive vorticity will link up with positive vorticity in the horse-shoe vortex.

Figure 4 presents the y-, and z-components of vorticity and pressure, at a given instance in time in the x-y plane corresponding to z/d=0.137. The corresponding x-component of vorticity was provided earlier in Fig. 3. The y-component of vorticity shows the signature of the horseshoe vortex beginning roughly 1-diameter upstream of the jet exit, but diminishes rapidly downstream of x/d=0, implying the reorientation of the vortex by the crossflow. The large positive vorticity values from the trailing edge of the hole are also evident and are associated with the boundary layer on the trailing wall of the jet exit. The corresponding negative vorticity along the leading edge of the jet hole is considerably smaller due to the distortion of the jet-hole exit profile by the crossflow (as obtained from measurements) which diminishes the velocity gradients along the leading edge and accentuates them along the trailing edge. Downstream from the hole, patches of negative vorticity can be observed. These are presumably associated with the jet-shear-layer or ring vortices associated with Kelvin-Helmholtz rollup.

The z-vorticity trace shows two distinctive features. First, the horseshoe vortex is associated with positive z-vorticity downstream of the leading edge of the injection hole. This is presumably induced by the periodic splitting and transverse entrainment of the vortex into the wake region. The vortex is therefore not only rotating in the y-z (cross-stream plane), but also in the x-y plane. The second distinctive feature is associated with the wake region where patches of strong positive and negative z-vorticity is noted. The negative vorticity is associated with the wake vortex, and Kelso et al. (1996) and Fric and Roshko (1994) have concluded that this is caused by the entrainment of the crossflow boundary layer into the wake, and its reorientation by the vertical upflow. Further evidence and clarification on this will be provided in Figs. 6 and 7. Three mechanisms for the positive vorticity are possible. First, an examination of the jet-hole-exit profile shows strong pockets of z-vorticity, and these could be transported downstream into the wake region. Second, the periodic entrainment of the horse-shoe vortex (discussed in reference to Fig. 3), associated with positive z-vorticity as noted above, can lead to pockets of positive z-vorticity in the wake. Third, Kelso et al. (1996) have postulated a mechanism for wake vortices, where the "upright vortices are formed by vortex loops on either side of the wake", and is "composed of vorticity from one or the other side of the wake". Such a mechanism would lead to alternate positive and negative packets of vorticity. While, at the z/d=0.137 location, the wake vortices appear to be contiguous, at a higher z/d location (z/d=0.42), the vortices are more distinct and separate from each other. The visualization pictures of Fric and Roshko (1994) and Kelso et al. (1996) appear to indicate that such behavior is also borne out in the experiments.

The pressure contours show the stagnation region upstream of the jet centerline, and the region of low pressure just downstream of the leeward side of the jet. Because of the low blowing ratio (0.5), the stagnation region extends into the jet-exit-hole . The lower pressures in the horseshoe vortex and its trajectory is clearly evident. The excursions of the crossflow boundary layer or the horse-shoe vortex into the low pressure wake region are also noticeable in the form of spanwise fingering of the pressure contours originating from the crossflow regions. The adverse pressure gradient regions near

the jet center plane that lead to the wall vortex system can also be seen in the pressure contours.

Dynamics of the Large Scale Structures

In the discussion below we will focus attention on the vorticity and pressure contours at different streamwise (x-y and x-z) and cross-stream (y-z) planes. Of interest is the dynamics of the structures, and therefore, results are presented for successive times. In picking the time increments and the time interval over which the data is to be presented, a random sampling of a few locations was made, and a Fast Fourier Transform (FFT) of the time-trace of the velocity variables at that location was performed. A range of frequencies were obtained , representing different scales in the flow. An estimate of a dominant mode was made, and the time-period of this mode was used to make a decision on the time interval over which the data is to be presented. A representative increment in time of $9x10^{-4}$ or $18x10^{-4}$ seconds over this interval was then picked to illustrate the temporal evolution.

Figures 5, 6, and 7 show the x-vorticity together with the superimposed velocity vectors in three streamwise locations, corresponding to x/d=0 (jet center plane), x/d=1 (near-wake region), and x/d=4 (far-wake region). Figures 8, 9, and 10 show the corresponding pressure contours.

At the low blowing ratio value of 0.5, the jet begins to bend immediately. Therefore the CVP is established early in the jet development. At x/D=0, the velocity vectors indicate the stretching of the core jet by the crossflow and by the bound vorticity in the jet-exit profile. Early evidence of the development of the CVP can be seen in the region directly above the jet associated with a pocket of negative vorticity. The negative vorticity exiting the transverse edge of the jet hole is seen to be primarily transported in the transverse direction directly below the horse-shoe vortex system, and serves to strengthen the horseshoe vortex. This was also observed at the z/d=0 plane in Fig. 3, and as noted earlier is associated with the pressure defect established between the high pressure region in the middle of the hole (associated with the stagnation region created when the jet encounters the crossflow) and the low pressure regions associated with the wake. The cross-stream pressure profile in Fig. 8 shows that there are two regions of low pressure in the transverse direction, one associated with the jet-exit-flow boundary layer, and the other associated with the horse-shoe vortex. In between there is a region of adverse pressure gradient, but no instantaneous flow reversals were noted. With time, the low pressure region associated with the horse-shoe vortex (Fig. 8) and the eye of the vortex (Fig. 5) meanders somewhat in the transverse direction first moving toward the jet center plane and then away from it. As seen in Fig. 3 and also in Fig. 5, the horse-shoe vortex is a dominant feature in this flow, and at certain time instances, the positive vorticity associated with this system extends all the way to the transverse edge of the jet.

At x/d=1 (Figs. 6 and 9), corresponding to the near-wake region, the CVP (negative vorticity) is more well-defined. However, as noted in Fig. 3, it is convoluted with patches of positive vorticity, which are a consequence of the entrainment of the crossflow boundary layer and fluid from the horse-shoe vortex system into the wake. This is clearly evident at time instances marked as $27x10^{-4}$, $36x10^{-4}$, $45x10^{-4}$, and $54x10^{-4}$ seconds. The flow is entrained into the wake along a thin stream adjoining the plate surface, and separates near the jet center plane forming a recirculation or wall vortex with positive vorticity just below the CVP. As can be seen clearly at $27x10^{-4}$, $36x10^{-4}$, and $45x10^{-4}$ seconds, this wall vortex is entrained by the upflow into the CVP. As the z-vorticity contours will show later, the entrained wall vortices (with x-vorticity) are reoriented into upright wake vortices (with z-vorticity). Note that unlike the high blowing ratio (in the range of 2 to 10) cases considered by Fric and Roshko (1994) and Kelso et al. (1996), at the low blowing ratio considered in this study, the CVP is close to the surface, and therefore the upflow entrainment of the wall vortices

significantly convolutes the CVP. Another important observation is that at certain time instances (see $36x10^{-4}$ seconds), part of the fluid in the horse-shoe vortex system is entrained along with the crossflow into the wake. This can be even more clearly observed at x/d=4.

The CVP can also be observed to go through a sequence of being pinched off at the top resulting in a separate region of negative vorticity above the CVP (see the contours at $18x10^{-4}$ seconds), and then reconnecting later (see the contours at $54x10^{-4}$ seconds). In examining the pressure contours (Fig. 8), this pinch off is associated with the development of a local pressure excursion near the top of the CVP. In the vicinity of the jet center-plane, adverse pressure gradients in the transverse direction can clearly be seen, which as discussed above, leads to the development of the wall-vortex. Associated with this, favorable pressure gradients can be seen in the vertical direction leading to the upward entrainment of the wall vortex.

At x/d=4, the CVP has grown in size considerably, and its various dynamical features are illustrated in Fig. 7. At t=0 sec, the CVP has two regions of concentrated vorticity, and there is significant entrainment of the crossflow into the region directly below the CVP leading to a wall vortex. However, over more than half the transverse direction along the wall, there is an adverse pressure gradient (Fig. 10) leading to a thin, elongated wall vortex, much unlike that seen in the near wake region. Further, the entrainment and reorientation of the wall vortex is much more complex. At certain time instances, the crossflow is directly entrained into the mid-regions of the CVP (at z/d nearly equal to 0.5) made possible by mildly favorable pressure gradients in the transverse direction (see pressure contour at $18x10^{-4}$ seconds) at this level. However close to the jet center plane, the pressure gradient becomes adverse, leading to the formation of a mid-span vortex with positive vorticity. This mid-span vortex splits the primary CVP into two halves. As the mid-span vortex is entrained upwards, the two halves of the CVP reconnect behind it. At $36x10^{-4}$ seconds, the pressure contours show a strong pressure deficit associated with the positive vorticity vortex, with high pressure regions on either side. A fairly large positive vorticity eddy is therefore obtained, centered near z/d=1, and appears nestled between the two legs of the CVP (each driven by the high pressure region on either side of the pressure deficit). The right lobe of the CVP then diminishes (as does the high pressure region driving it), the positive vorticity eddy (and the associated low pressure region) descends to take its place connecting with the wall vortex, and the left lobe of the CVP is accentuated. The CVP continues to develop around the positive vorticity eddy as it is entrained upwards. At $63x10^{-4}$ seconds, pieces of the positive vorticity eddy are entrained into the CVP which takes on an inverted -E shape.

The horse-shoe vortex can be seen to be lifted off the surface, and at specific time-instances (see $27x10^{-4}$ seconds) develops a tail that connects with the wall vortex along the jet center-plane. In this instance the wall vortex is fed both by the crossflow boundary layer and by the horse-shoe vortex. The eye of the horse-shoe vortex bobs up and down along the right symmetry plane, and as it moves up the cross-flow is entrained beneath it. However, in a manner similar to that along the jet center plane, the entrained fluid encounters an adverse pressure gradient, and a wall vortex is also obtained directly beneath the horse-shoe vortex. To the authors knowledge, observations of a wall vortex on the horse-shoe side has not been reported in the literature.

Figure 11 shows the z-vorticity in an x-y plane at z/d=0.42. Also shown are superimposed velocity vectors. The footprint of the horse-shoe vortex near its evolution upstream of the exit-hole center and in the far wake regions can be quite clearly seen. Near the stagnation region associated with the evolution of the vortex, pressure decreases away from the jet center plane, and leads to negative vorticity of the horseshoe vortex. Near the opposite transverse boundary, pressure decreases as one moves away from that boundary, leading to a

positive z-vorticity of the horseshoe vortex. In the wake, both positive and negative vorticity eddies are observed, with the negative vorticities associated with the upright vortices arising either from a reorientation of the wall vortices or from a reorientation of the mid-span vortices. Three possible reasons for the positive vorticity eddies were mentioned earlier. It should be noted that contiguous packets of negative upright vortices are possible, as shown at t= $36x10^{-4}$ seconds. A careful examination of frame-by-frame evolution indicates that vortex stretching and breakup, and compression and coalescence are occurring at several time instances. The velocity vectors not only show significant entrainment of the crossflow into the wake region, but also show stagnation regions. These are associated with the reorientation of the wall or mid-span vortex into an upright vortex. Note also the existence of neighboring eddies rotating in the same direction.

Figure 12 shows the y-vorticity contours in a x-z plane corresponding to y/d=0.45. The positive vorticity along the downstream edge of the coolant hole, and the negative vorticity along the upstream edge are evident, and are associated with the jet-hole exit velocity profiles. Clear evidence of shear-layer vortices can be seen on the leeward side of the jet. These vortices are shed from both sides of the jet, but convect downstream at different velocities, with the windward vortices (negative vorticity) accelerated by the high-speed crossflow. It appears that the crossflow strips the shear layer vorticity from the windward and leeward sides (negative and positive vorticity respectively). Vortex pairs of positive vorticity and negative vorticity can be seen at t=0 seconds. One vortex is along the wall, and the other is along the underside of the deflected jet. These vortex pairs can clearly be seen to undergo pairing events. For example, at t=0 seconds, between x/d of 1.25 and 2.5, four vortex pairs can be distinctly observed. These four pairs can be clearly observed to have paired at t=$18x10^{-4}$ seconds, and have convected downstream to the region between x/d of 1.25 and 2.75. With time, these vortices are stretched and grow downstream. It is anticipated that some reorientation of these vortices in the streamwise direction is achieved by the crossflow. This reorientation, depending on the initial vorticity direction, can either enhance or detract the CVP.

The superimposed velocity vectors clearly show the positive vorticity near the wall directing the fluid downward in a sweep-type motion, and the negative vorticity near the wall ejecting the fluid upward from the surface. Thus the wall is subject to alternate sweep and ejection events, which can lead to high levels of wall shear.

Comparison with Experiments

The time averaged x and y components of velocity at various locations is shown in Figure 13. It is compared to the experimental data of Ajersch et al (1995). Agreement with Ajersch et al (1995) is quite good in the near jet region but deteriorates somewhat as one moves downstream away from the jet. One possible reason for this is the grid spacing which becomes progressively coarser as one moves downstream away from the jet and the increasing importance of the small scales further downstream.

CONCLUDING REMARKS

A time-and space- accurate computational study is performed to understand the dynamics of the large scale structures in the near field of a film cooling jet injected normal to a crossflow. The following are the major conclusions of this study.

1. The near-field is characterized by several, fairly dominant dynamical large scale structures. These include the CVP, shear-layer vortices, horse-shoe vortices, wall vortices and wake vortices.

2. The CVP appears to be a dynamically-convoluting structure with patches of positive and negative vorticity. The convolution appears to stem from the low blowing ratio, due to which the CVP

is constrained to the near wall region. The crossflow is entrained periodically into the CVP and leads to the convolution.

3. The crossflow and flow from the horse-shoe vortex system are both observed to be entrained into the wake region. The entrained near-wall crossflow-boundary layer experiences an adverse pressure gradient near the jet symmetry plane and separates to form a wall vortex. This wall vortex is then stretched and reoriented into the upright wake vortices.

4. Direct entrainment of the mid-span crossflow into the wake region is also observed for x/d=4. This mid-span vortex (with x-vorticity) dynamically interacts with the CVP, the wall vortices, and also the horse-shoe vortex system. The CVP is seen to undergo a process of bifurcation and reconnection.

5. The horse-shoe vortex appears to be a dominant feature for a normal jet in crossflow. Bifurcation of the horse-shoe vortex, and its entrainment into the wake region is clearly evident.

6. The wake vortices (z-vorticity) are an outcome of the reorientation of the wall vortices and the mid-span vortices by the wake upflow.

7. The shear layer vortices (y-vorticity)appear primarily on the leeward side of the jet. This is attributed to the low blowing ratio case being studied here. The crossflow appears to strip the y-vorticity from the windward and leeward sides for the jet into the wake region. Vortex pairs are clearly observed to undergo pairing and stretching events.

8. Comparisons of the current predictions with the mean velocity measurements are in good agreement in the near-field.

ACKNOWLEDGMENTS

This work was supported by a grant from the Turbomachinery Physics Group at NASA-Lewis. Dr. Chi Wang and Dr. Ray Gaugler served as the technical monitors for the project. Their support is gratefully acknowledged. Computing support for the project was received from NASA-Ames Computing Center and also through NASA-Lewis. This support is also acknowledged. The assistance of Dr. Albert Harvey III and Raymond Jones at Dow Chemical Company is gratefully acknowledged.

REFERENCES

Ajersch,P.,Zhou,J.M.,Ketler,S.,Salcudean,M. and Gartshore ,I,S. 1995 "Multiple Jets in a Crossflow : Detailed measurements and Numerical Simulations" ,*Trans. ASME*

Andreopoulos J. 1985 "On the structure of jets in a crossflow" J.Fluid Mech. vol. 157

Andreopoulos J. and Rodi W. 1984 "Experimental investigation of jets in a crossflow" *J.Fluid Mech.* vol. 138

Chorin, A. J. 1968 "Numerical Solution of the Navier-Stokes Equations", *Math. Comput.*, vol. 22, pp.745-762

Crabb D., Durao D.F.G., Whitelaw 1981 "A round jet normal to a crossflow" *Transactions of the ASME*, Vol. 103 March

Demuren A.O. 1993 "Characteristics of three-dimensional jets in crossflow" *Int. J. Engng Sci.* Vol 31 No. 6, pp.899-913

Fornberg B. G. 1988 "Generation of finite difference formulas on arbitrarily spaced grids" *Mathematics of Computations* vol. 31 Number 184 October pp. 699-706

Foss, J. 1980" Interaction region phenomena for the jet in a cross-flow problem" *Rep. SFB 80/E/161, Univ. Karlsruhe*

Fric T. F., & Roshko A. 1994 "Vortical structure in the wake of a transverse jet" *J. Fluid Mech.* vol. 279, pp. 1-47

Garg, V. K., & Gaugler R. E., 1995 "Effect of velocity and temperature distribution at the hole exit on film cooling of turbine blades", ASME paper 95-GT-2

Garg, V. K., & Gaugler R. E., 1994 "Prediction of film cooling on gas turbine airfoils", ASME paper 94-GT-2

Ho, C. M., & Huerre, P., 1984 "Perturbed Shear Layers" *Ann. Rev Fluid Mech.*, vol 16 pp.365-424

Hyams D. G., Leylek J. H. 1997 "A detailed analysis of film-cooling phsyics, Part III: streamwise injection with shapedl holes" *ASME Paper* 97-GT-269

Jones, W. P. & Wille, M. 1996 "Large eddy simulation of a round jet in crossflow" *Engineering Turbulence Modeling and Experiments* 3. Ed. Rodi, W. and Bergeles, G. pp.199-209

Kelso R. M., Lim T.T., and Perry A. E. 1996 "An Experimental Study of Round Jets in Cross-Flow", *J.Fluid Mech.* vol. 306 pp. 111-144

Kim, S.W., & Benson, T. J. 1992 "Calculation of a circular jet in crossflow with a multiple-time-scale turbulence model" *Int. J. Comp. Phys.* vol 59. pp. 308

McGovern T. K., Leylek J. H. 1997 "A detailed analysis of film-cooling phsyics, Part II: compound-angle injection with cylindrical holes" *ASME Paper* 97-GT-269

Moussa Z. M., Trischka J. W. and Eskinazi S. 1977 "The near field in the mixing of a round jet with a cross-stream" *J.Fluid Mech.* vol. 80 pp. 49-80

Patankar, S. V. Basu, D. K. & Alpay, S. A., 1977 "Prediction of the three-dimensional velocity field of a deflected turbulent jet" *Trans. SME I: J. Fluids Engng* 99, pp. 758-762

Rogers, S., Kwak, D. 1991 "Steady and Unsteady Solutions of the Incompressible Navier-Stokes Equations", *AIAA Journal*, Vol. 29, Nov 4, pp. 603-610

Singer B.A. 1994 "Metamorphosis of a hairpin vortex into a young turbulent spot" *Phys. Fluids* 6 (11) Nov.

Sykes, R. I., Lewellen, W. S. & Parker, S. F. 1986 "On the vorticity dynamics of a turbulent jet in a crossflow" *J. Fluid Mech.* vol. 80, pp. 49-80

Yuan L.L., Street, R. L. 1996 "Large Eddy Simulation of a Jet in Crossflow" *ASME Fluids Engineering Division* Vol. 242

Walters D. K., Leylek J. H. 1997 "A detailed analysis of film-cooling phsyics, Part I: streamwise injection with cylindrical holes" *ASME Paper* 97-GT-269

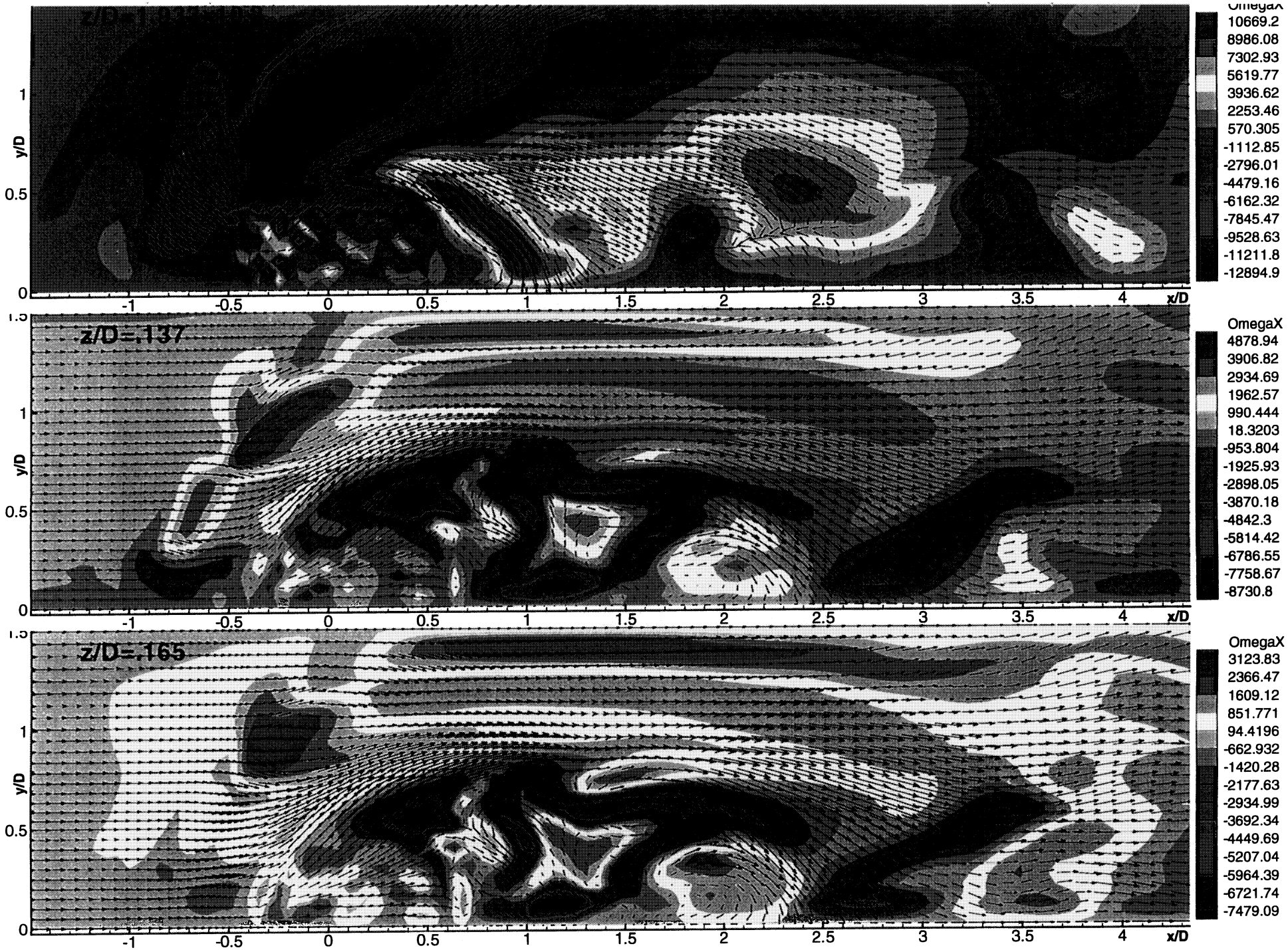

FIGURE 3 X COMPONENT OF VORTICITY IN THE XY PLANE AT ONE INSTANT IN TIME

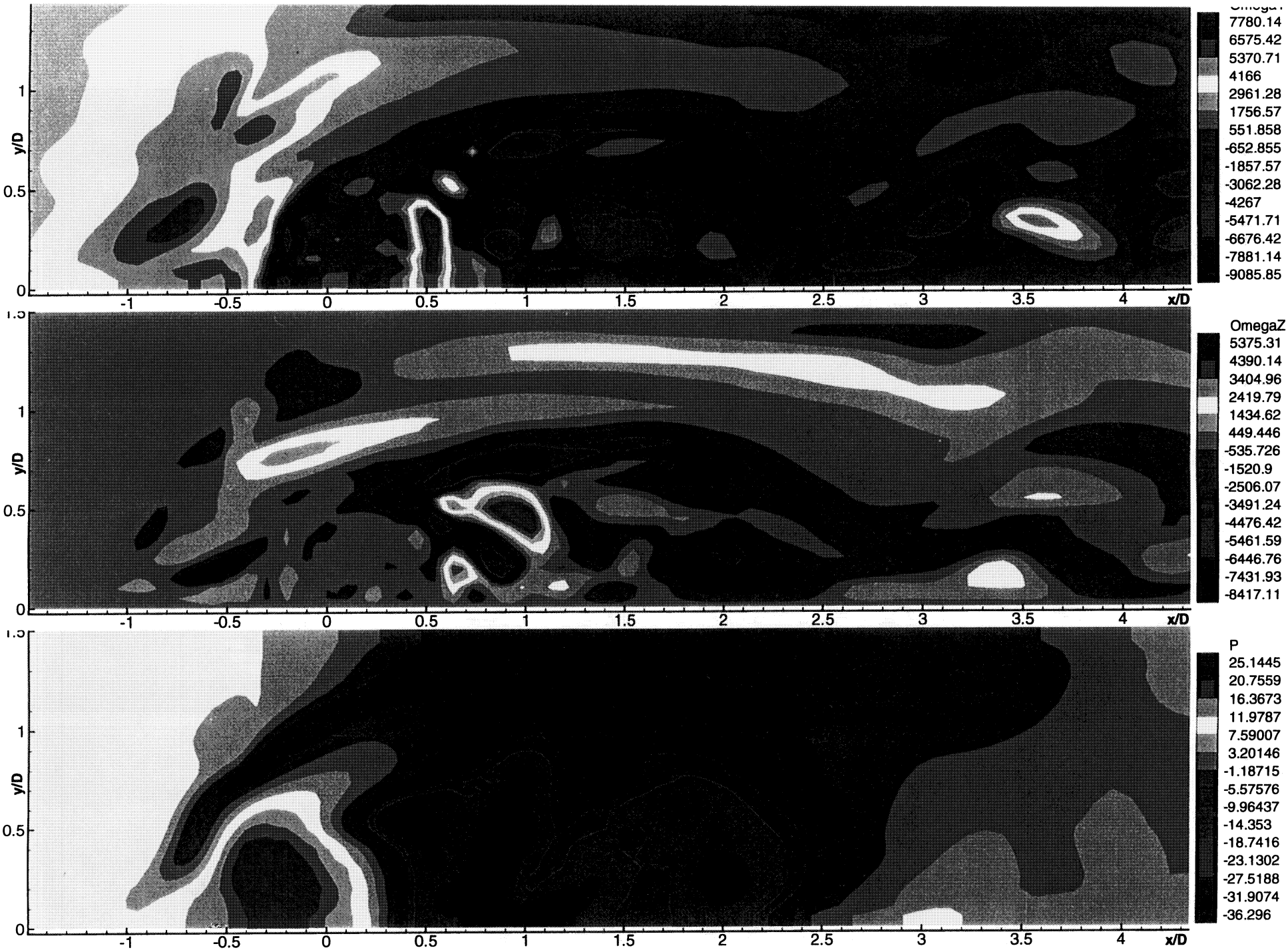

FIGURE 4 Y AND Z COMPONENTS OF VORTICITY AND PRESSURE IN THE XY PLANE AT THE SAME INSTANT IN TIME AT Z/D=.137

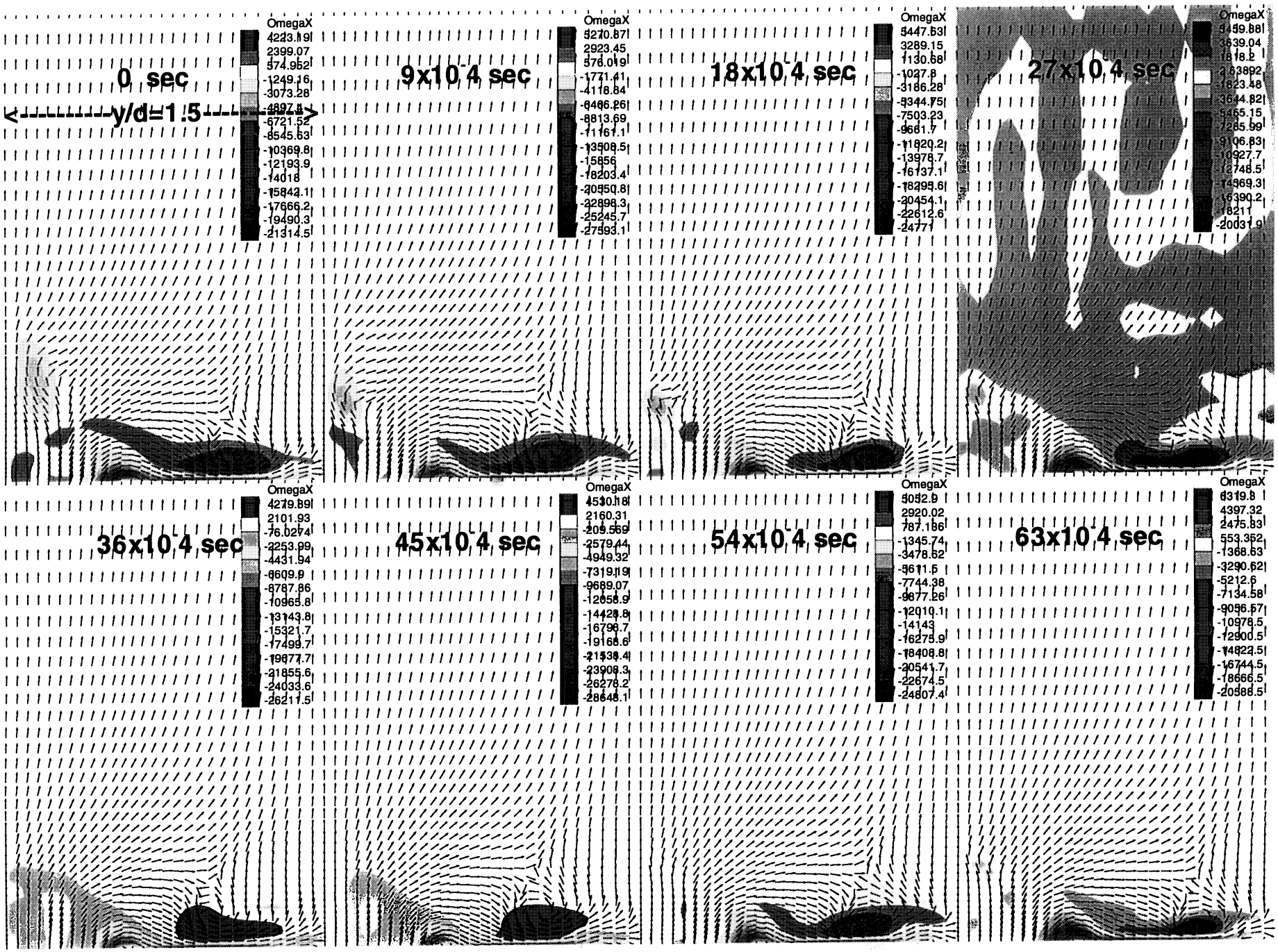

FIGURE 5 X COMPONENT OF VORTICITY AND VELOCITY VECTORS IN THE YZ PLANE AT X/D=0

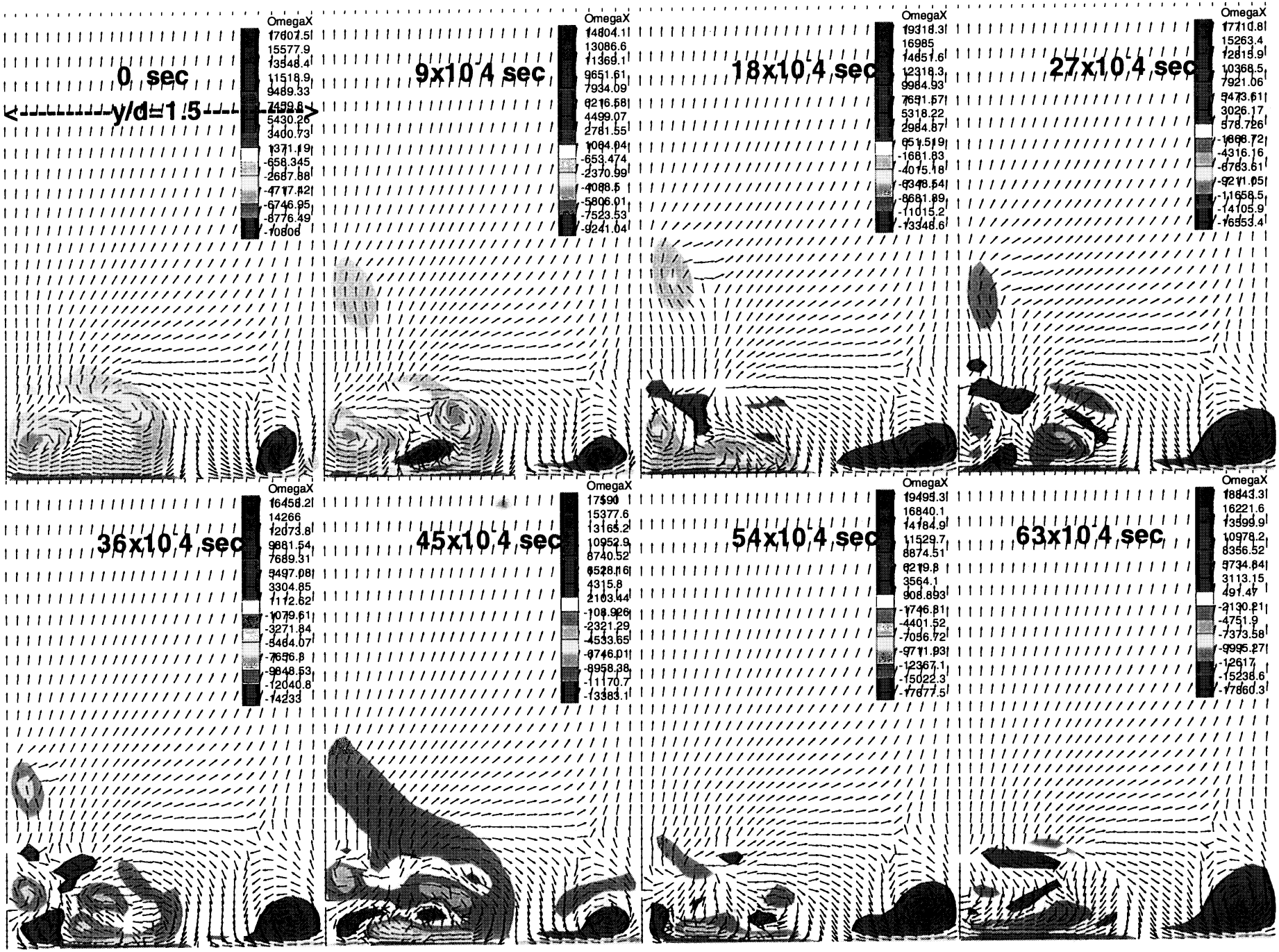

FIGURE 6 X COMPONENT OF VORTICITY AND VELOCITY VECTORS IN THE YZ PLANE, AT X/D=.97!

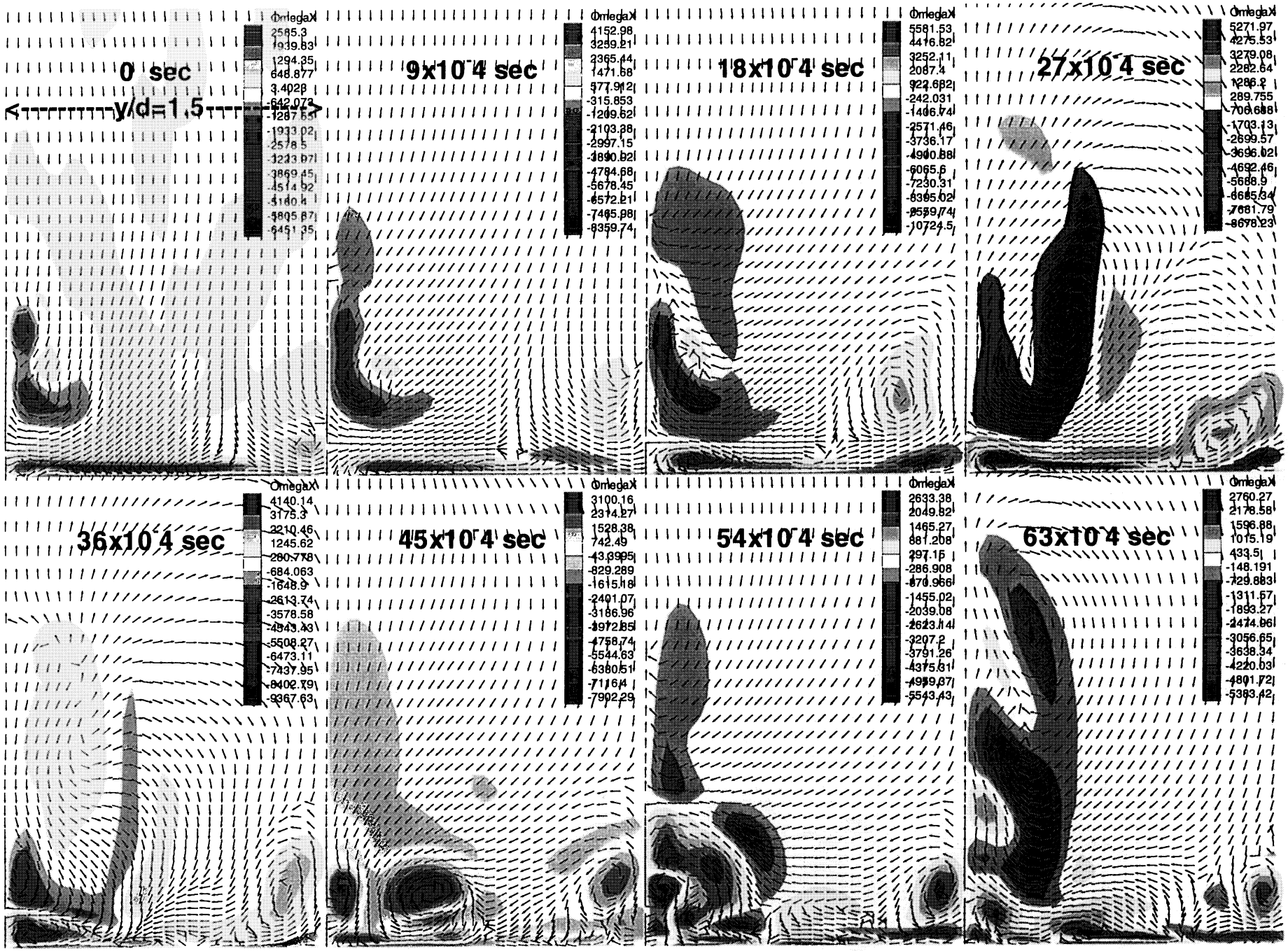

FIGURE 7 X COMPONENT OF VORTICITY AND VELOCITY VETCORS IN THE YZ PLANE, AT X/D=4.0

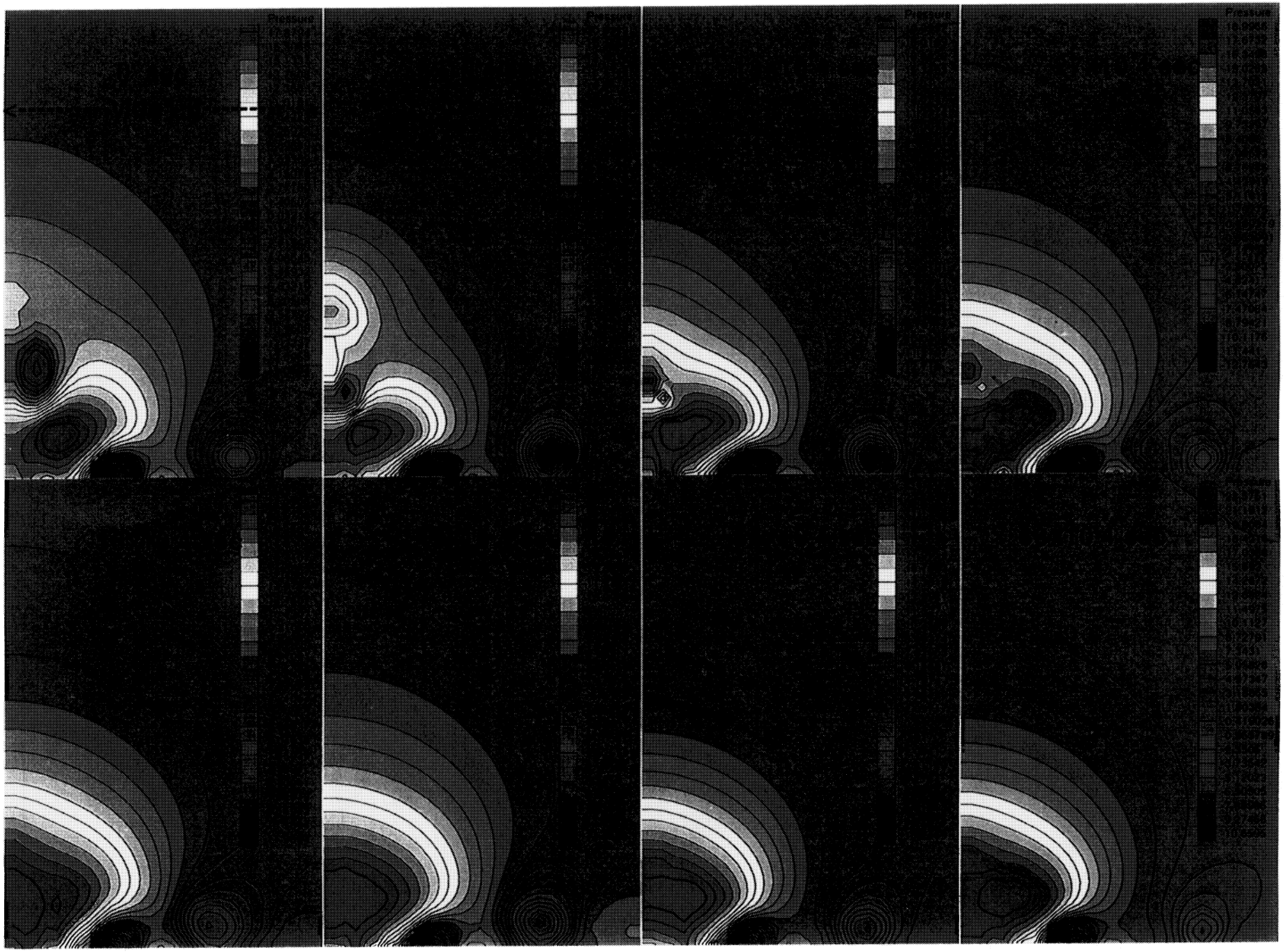

FIGURE 8 PRESSURE IN THE YZ PLANE, AT X/D=0

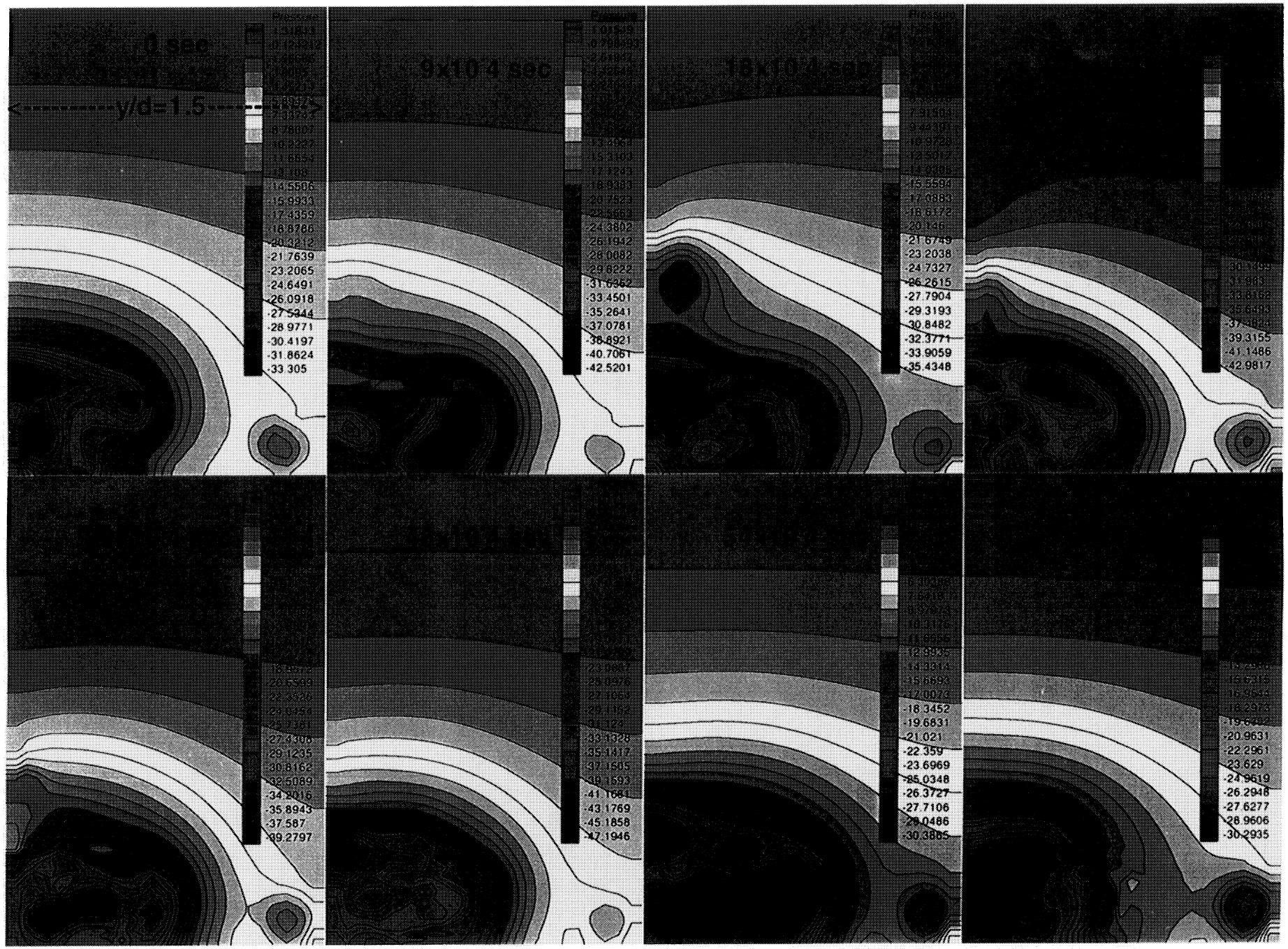

FIGURE 9 PRESSURE IN THE YZ PLANE, AT X/D=.979

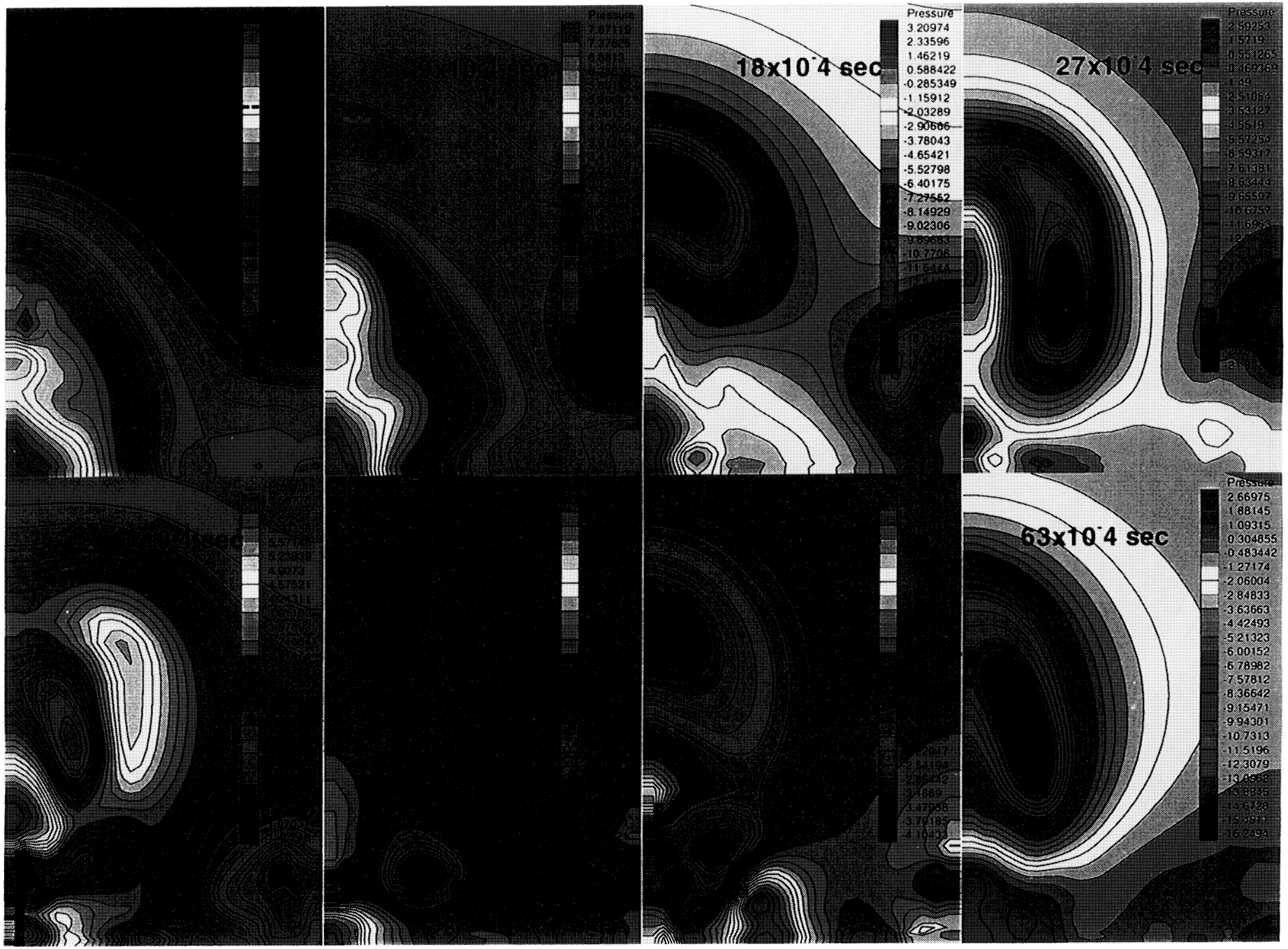

FIGURE 10 PRESSURE IN THE YZ PLANE, AT X/D=4.047

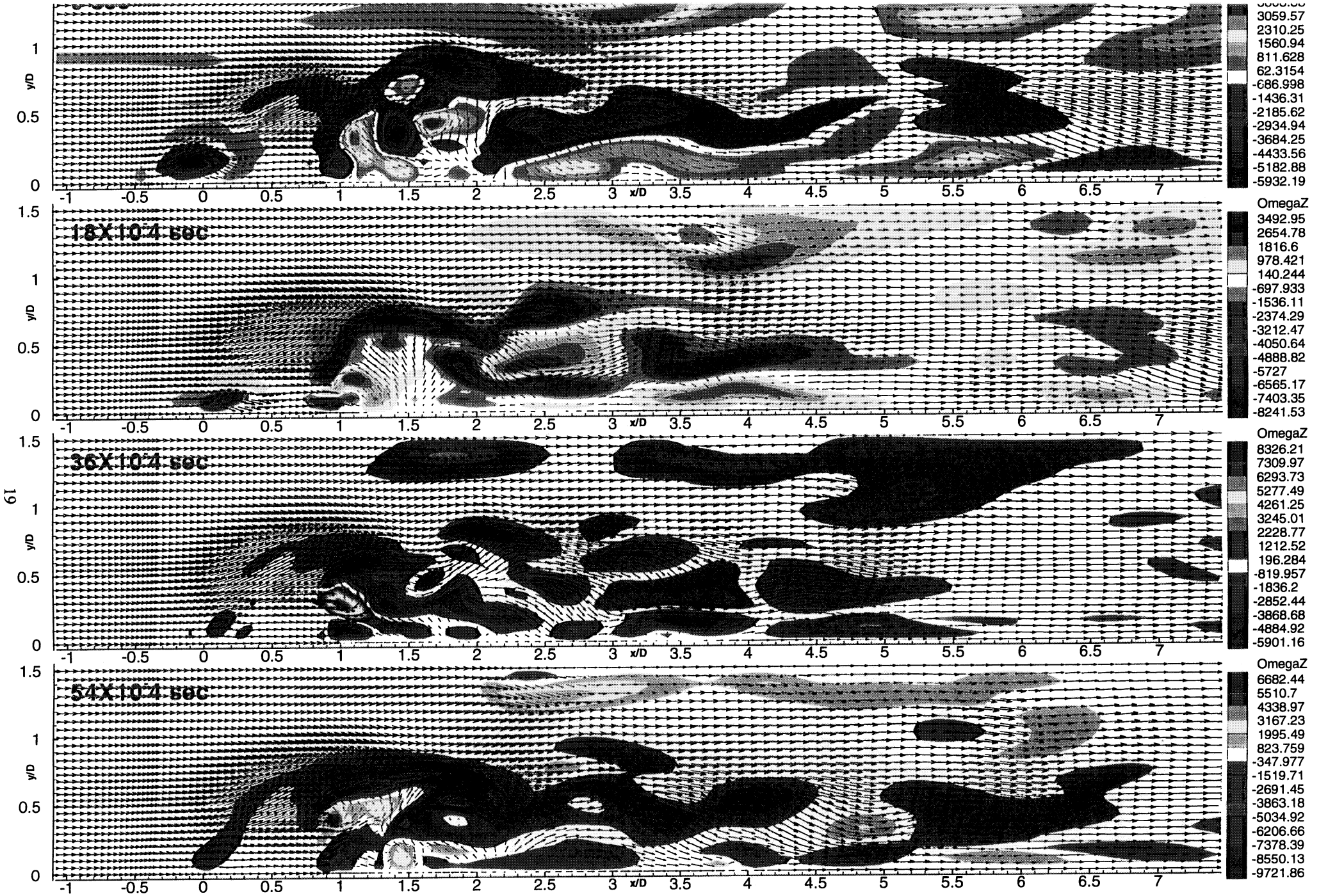

FIGURE 11 Z COMPONENT OF VORTICITY IN THE XY PLANE AT Z/D=.42

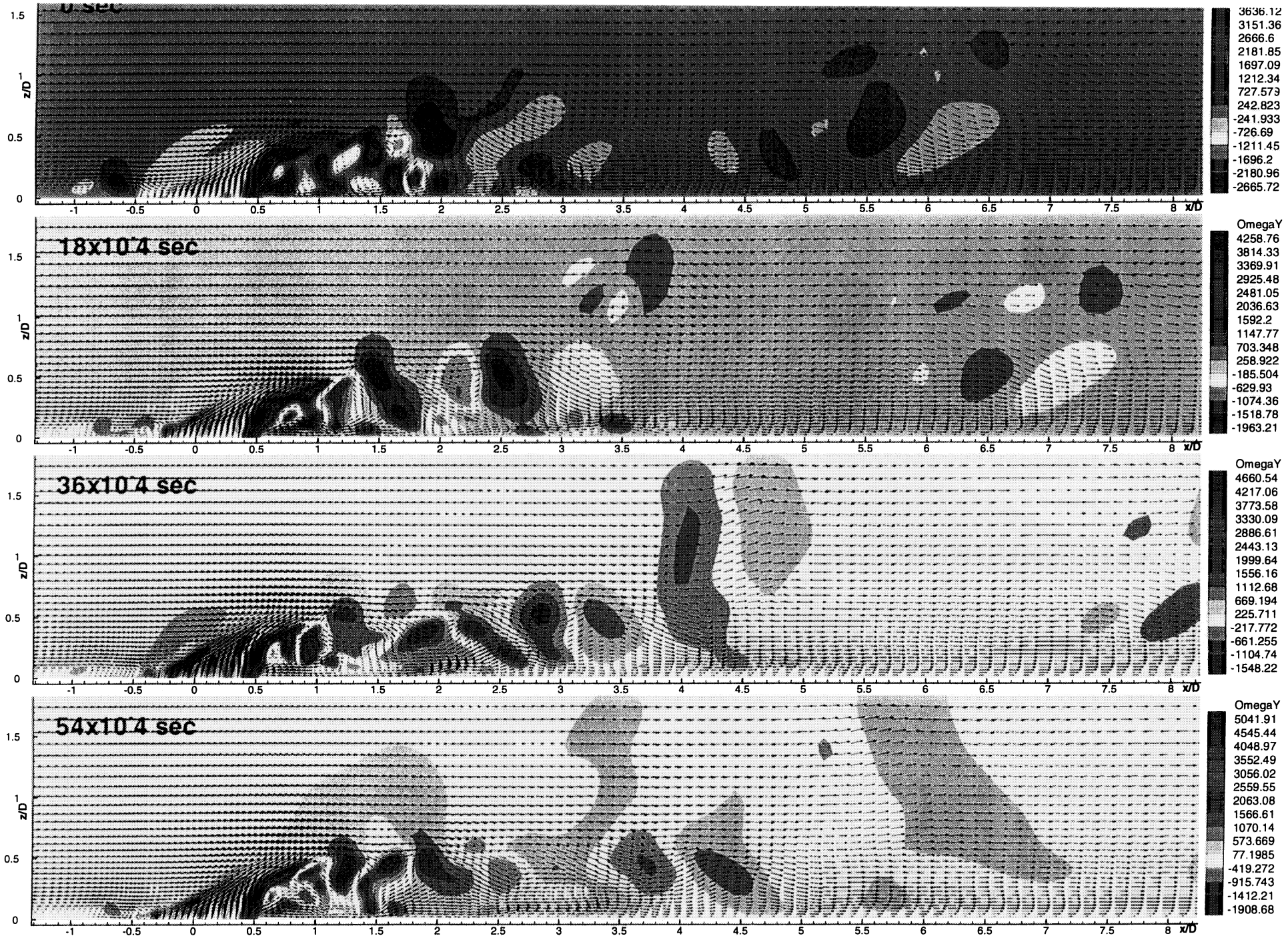

FIGURE 12 Y COMPONENT OF VORTICITY AND VELOCITY VECTORS IN THE XZ PLANE AT Y/D=.45

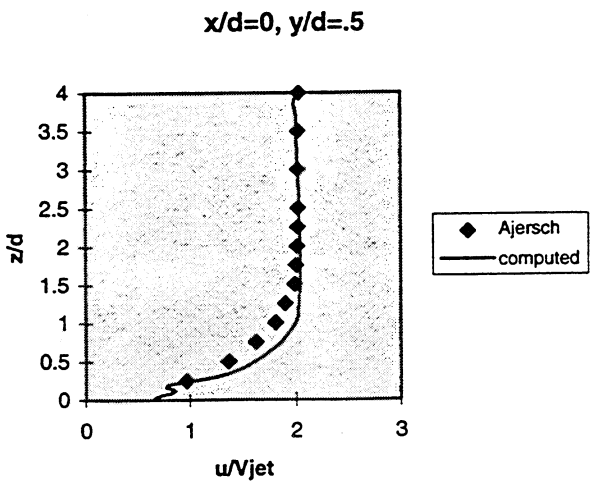

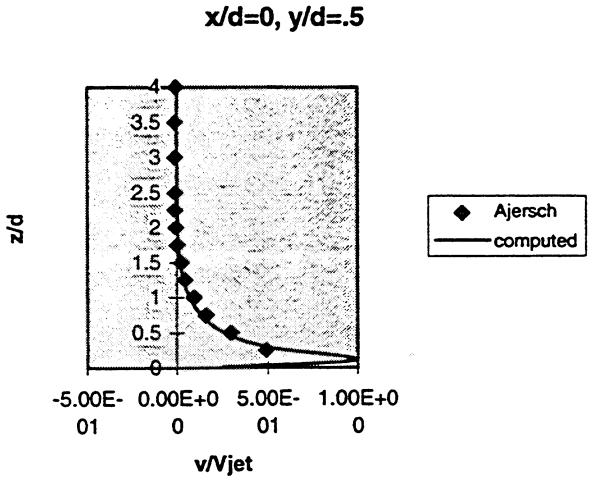

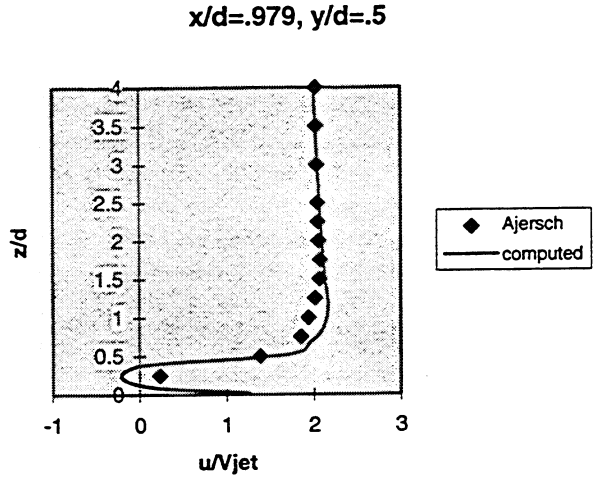

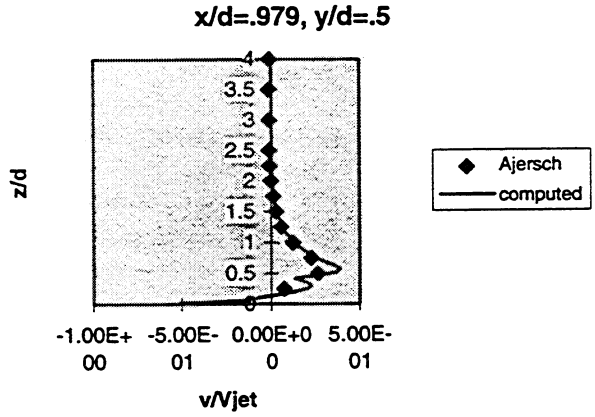

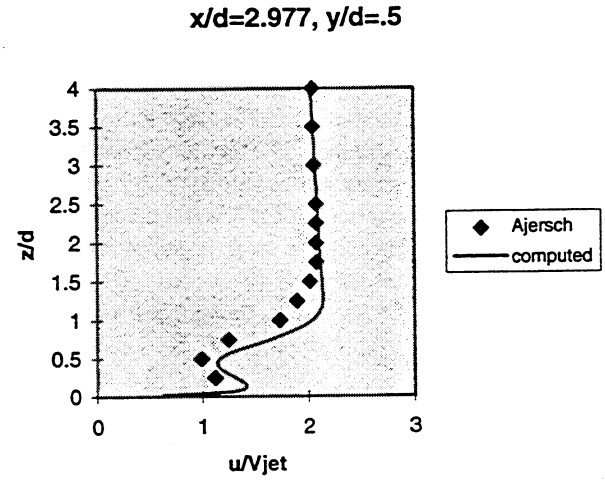

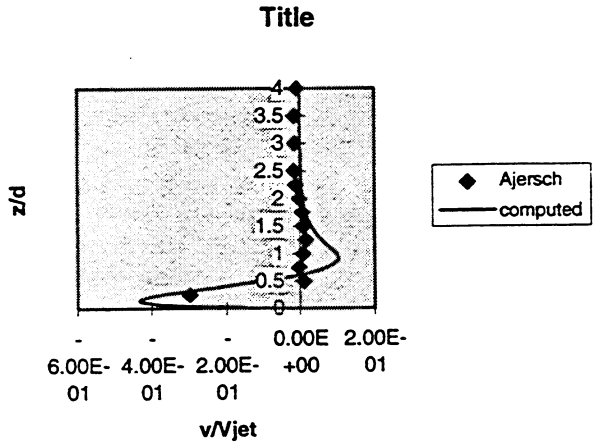

FIGURE 13 TIME AVERAGED X AND Y COMPONENTS OF VELOCITY

REPORT DOCUMENTATION PAGE

Form Approved
OMB No. 0704-0188

1. AGENCY USE ONLY (*Leave blank*)	2. REPORT DATE	3. REPORT TYPE AND DATES COVERED
	March 1998	Final Contractor Report

4. TITLE AND SUBTITLE

Dynamics of Large-Scale Structures for Jets in Crossflow

5. FUNDING NUMBERS

WU–538–12–10–00
NAG3–1641

6. AUTHOR(S)

Frank Muldoon and Sumanta Acharya

7. PERFORMING ORGANIZATION NAME(S) AND ADDRESS(ES)

Louisiana State University
Mechanical Engineering Department
Baton Rouge, Louisiana 70803

8. PERFORMING ORGANIZATION REPORT NUMBER

E–11125

9. SPONSORING/MONITORING AGENCY NAME(S) AND ADDRESS(ES)

National Aeronautics and Space Administration
Lewis Research Center
Cleveland, Ohio 44135–3191

10. SPONSORING/MONITORING AGENCY REPORT NUMBER

NASA CR—1998-206606

11. SUPPLEMENTARY NOTES

Prepared for the 43rd Gas Turbine and Aeroengine Congress, Expo, and User's Symposium sponsored by the International Gas Turbine Institute of the American Society of Mechanical Engineers, Stockholm, Sweden, June 2–5, 1998. Project Manager, Raymond E. Gaugler, Turbomachinery and Propulsion Systems Division, NASA Lewis Research Center, organization code 5820, (216) 433–5882.

12a. DISTRIBUTION/AVAILABILITY STATEMENT

Unclassified - Unlimited
SubjectCategories: 02, 07, 34, and 64 Distribution: Nonstandard

This publication is available from the NASA Center for AeroSpace Information, (301) 621–0390.

12b. DISTRIBUTION CODE

13. ABSTRACT ***(Maximum 200 words)***

Results of a three dimensional unsteady computational study of a row of jets injected normal to a cross-flow are presented with the aim of understanding the dynamics of the large scale structures in the region near the jet. The jet to cross-flow velocity ratio is .5. A modified version of the computer program (INS3D) which utilizes the method of artificial compressibility is used for the computations. Results obtained clearly indicate that the near field large scale structures are extremely dynamical in nature, and undergo bifurcation and reconnection processes. The dynamical near field structures identified include the counter rotating vortex pair (CVP), the horse-shoe vortex, wake vortex, wall vortex and the shear layer vortex. The dynamical features of these vortices are presented in this paper. The CVP is observed to be a convoluted structure interacting with the wall and horse-shoe vortices. The shear layer vortices are stripped by the crossflow, and undergo pairing and stretching events in the leeward side of the jet. The wall vortex is reoriented into the upright wake system. Comparison of the predictions with mean velocity measurements is made. Reasonable agreement is observed.

14. SUBJECT TERMS

Gas turbine; Turbulence; Computational fluid dynamics

15. NUMBER OF PAGES

27

16. PRICE CODE

A03

17. SECURITY CLASSIFICATION OF REPORT	18. SECURITY CLASSIFICATION OF THIS PAGE	19. SECURITY CLASSIFICATION OF ABSTRACT	20. LIMITATION OF ABSTRACT
Unclassified	Unclassified	Unclassified	